JOURNAL OF Applied Polymer SCIENCE

Synthesis, Characterization, and Thermal Curing of a Novel Polyhedral Oligomeric Octa(propargylaminophenyl)silsesquioxane

Haibo Fan, Jiyu He, Rongjie Yang
School of Materials, Beijing Institute of Technology, Haidian District, Beijing 100081, People's Republic of China

Correspondence to: J. He (E-mail: hejiyu@bit.edu.cn)

ABSTRACT: A novel polyhedral oligomeric octa(propargylaminophenyl)silsesquioxane (OPAPS, $(SiO_{1.5}C_6H_4NHCH_2C{\equiv}CH)_8$) was prepared from octa(aminophenyl)silsesquioxane and propargyl bromide. The chemical structure of OPAPS was characterized by Fourier transform infrared spectroscopy (FTIR), nuclear magnetic resonance, X-ray diffraction (XRD), high-performance liquid chromatography, gel permeation chromatography, differential scanning calorimetry, and thermal gravimetric analysis (TGA). The structure of the thermally cured polymer of OPAPS was characterized by FTIR, XRD, and TGA. It had good thermal stability. TGA demonstrated that the thermal decomposition temperatures (T_{d5}) of the cured OPAPS polymer in nitrogen and air were 455.6 and 458.8°C, respectively. The thermal curing reaction kinetics of OPAPS were studied and some kinetic parameters were obtained. © 2012 Wiley Periodicals, Inc. J. Appl. Polym. Sci. 000: 000–000, 2012

KEYWORDS: synthesis; curing of polymers; high temperature materials; kinetics; terminal alkynyl groups

Received 6 February 2012; accepted 19 March 2012; published online
DOI: 10.1002/app.37734

INTRODUCTION

Polyhedral oligomeric silsesquioxanes (POSS) are a type of three-dimensional, structurally well-defined cage molecule with the general formula $(RSiO_{1.5})_n$. The inorganic silica-like core is surrounded by organic groups and the cage size is about 1.5 nm.[1–5] Typical POSS derivatives have the structure of a cube-octameric framework covalently bonded with eight organic groups, one or more of which is reactive or polymerizable.[6] They have attracted considerable interest in recent years due to not only their high performance, which originates from the combination of advantages of the inorganic and organic components in these materials, but also the unique features derived from their nanometer-scale architecture.[6–10] POSS have proven to be excellent platforms for new hybrid materials,[11–14] homogeneous models for silica,[15,16] supports for organometallic catalysts,[17–19] biocompatible drug carriers,[20] and also as anion receptors.[21,22]

It is well known that siloxane-containing polymers possess some unique properties, including good flexibility, high heat resistance, excellent moisture resistance, and good electrical properties.[23] But there are only a few reports of the synthesis of a polymer with POSS units in the main chain in the literature.[2,24,25]

The cyclotrimerization of terminal alkynyl groups attracted our attention because it is a kind of metal-free polymerization.[23,26,27] Some metallic catalyst residues can be detrimental to the electronic and optical properties of polymers: for example, light emissions from conjugated polymers can be quenched by metallic traps.[28] The introduction of POSS units into a thermosetting acetylene resin in main chains will probably improve some properties and produce a high-performance organic–inorganic hybrid resin.[2,29]

Herein, octaaminophenylsilsesquioxane (OAPS) was used to synthesize octa(propargylaminophenyl)silsesquioxane (OPAPS) containing eight terminal alkynyl groups. A complete characterization of OPAPS was carried out. A thermally cured polymer of OPAPS was obtained and the curing kinetics were investigated using differential scanning calorimetry (DSC).

EXPERIMENTAL

Materials

Octaphenylsilsesquioxane (OPS, $Si_8O_{12}(C_6H_5)_8$, M = 1033.2, 97%) was purchased from Hybrid Plastics. Propargyl bromide was purchased from Alfa Aesar, China. Triethylamine, NaCl, Na_2SO_4, and solvents such as dimethyl formamide (DMF), tetrahydrofuran (THF), ethyl acetate and hexane were of analytical purity and purchased from Beijing Chemical Works, China.

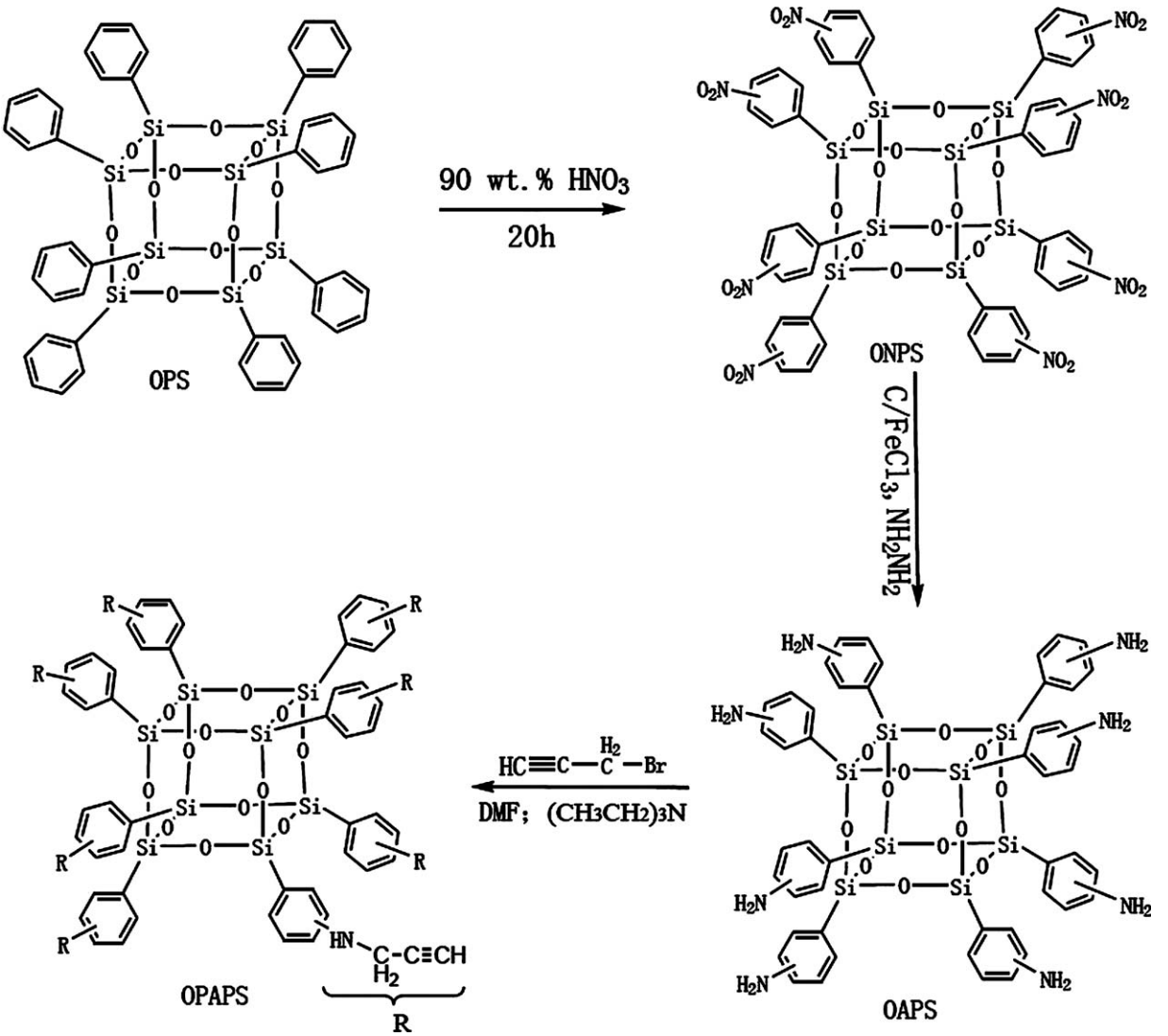

Scheme 1. Synthesis of OPAPS.

Synthesis of OAPS

OAPS was synthesized from OPS by following the literature method (Scheme 1).[30,31] OAPS: ^{1}H-nuclear magnetic resonance (NMR) spectroscopy (500 MHz, dimethyl sulfoxide (DMSO)-d_6, δ): 7.4–6.2 (2.0H, Ar H), 5.4–4.5 (1.0H, —NH_2); ^{29}Si solid NMR (400 MHz, δ): −68.3, −77.5; ^{13}C-NMR (500 MHz, DMSO-d_6, δ): 153.2, 147.9, 135.1, 131.4, 128.6, 121.2, 119.3, 116.4, 114.6, 113.3; Fourier transform infrared (FTIR) spectroscopy (KBr): ν = 3456 and 3358 (—NH_2), 1596 (C—H), 1115 (Si—O) cm^{-1}; Anal. Calcd. for OAPS: C 50. 0, H 4.16, N 9.71; found: C 48.9, H 4.38, N 9.31.

Synthesis of OPAPS

OAPS (0.5 g, 0.433 mmol, which is 3.46 mmol of —NH_2) and triethylamine (0.425 g, 4.21 mmol) were placed in a 100-mL three-necked round-bottomed flask equipped with a magnetic stirrer and a condenser; then DMF (20 mL) was added. The mixture was heated to 80°C under N_2, then propargyl bromide (80% in toluene, 1.56 g, 10.4 mol) was dissolved in DMF (5 mL) and added dropwise at 80°C within 15 min while it was stirred thoroughly. The color of the solution became deeper with the dropwise addition of propargyl bromide. The reaction mixture was continuously stirred at 80°C for 24 h, and then poured into an aqueous saturated solution of NaCl (100 mL). A deep yellow precipitate appeared and was collected. Then it was dissolved in THF (5 mL) and ethyl acetate (5 mL) and then washed with an aqueous saturated solution of NaCl (30 mL). The organic phase was dried over Na_2SO_4, then poured into hexane (100 mL). The precipitate was collected by filtration. The obtained powder was dried in a vacuum at 50°C.

The yield was 52.4% (Scheme 1). ^{1}H-NMR (500 MHz, DMSO-d_6, δ): 7.9–6.5 (3.81H, Ar H), 4.2–4.0 (0.54H, —NH—), 4.0–3.5 (1.84H, —CH_2—), 3.1–2.8 (1.00H, —C≡CH); ^{29}Si solid NMR (400 MHz, δ): −77.9; ^{13}C-NMR (500 MHz, DMSO-d_6, δ): 162.4, 146.9, 128.9, 124.3, 120.0, 79.5, 75.1; FTIR (KBr): 3288, 2113, 1697, and 642 (—C≡CH), 3375 (—NH—), 1115 (Si-O)

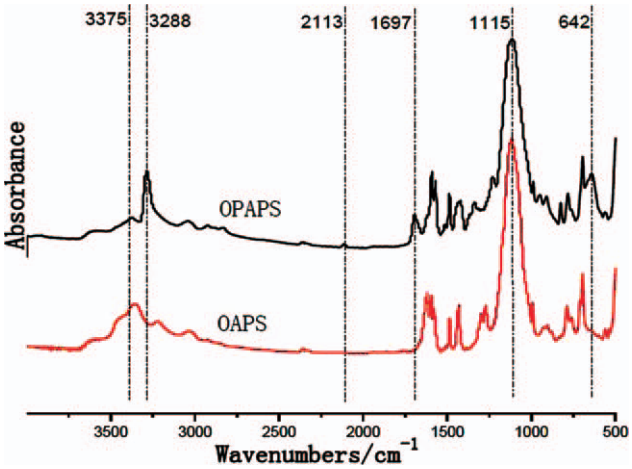

Figure 1. Fourier transform infrared spectra of OAPS and OPAPS (KBr). [Color figure can be viewed in the online issue, which is available at wileyonlinelibrary.com.]

cm^{-1}; Anal. Calcd for OPAPS: C 59.2, H 4.39, N 7.68; found: C 56.1, H 4.43, N 7.69.

Thermal Curing of OPAPS

The OPAPS was heated and kept in an oven at 150°C/1 h + 170°C/1 h + 190°C/2 h + 210°C/2 h + 230°C/2 h + 270°C/2 h + 320°C/3 h to get a thermally cured polymer under air. A piece of black solid was obtained. FTIR (KBr): 3375 (—NH—), 1115 (Si—O) cm^{-1}.

Characterization

FTIR spectra were recorded on a Nicolet 6700 IR spectrometer. The spectra were collected in 32 scans with a spectral resolution of 4 cm^{-1}.

^{1}H-NMR spectra and ^{13}C-NMR spectra were recorded on a Bruker Avance 500 NMR spectrometer operated in the Fourier transform mode. DMSO-d_6 was used as the solvent, and tetramethylsilane (TMS) was used as an internal reference.

^{29}Si solid NMR spectra were recorded on a Bruker Avance 400 NMR spectrometer.

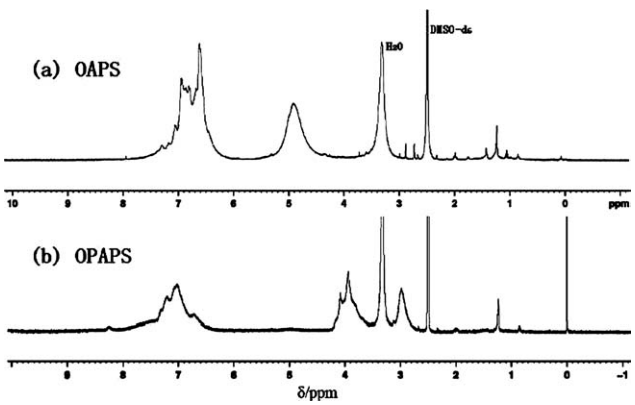

Figure 2. ^{1}H-NMR spectra of (a) OAPS and (b) OPAPS.

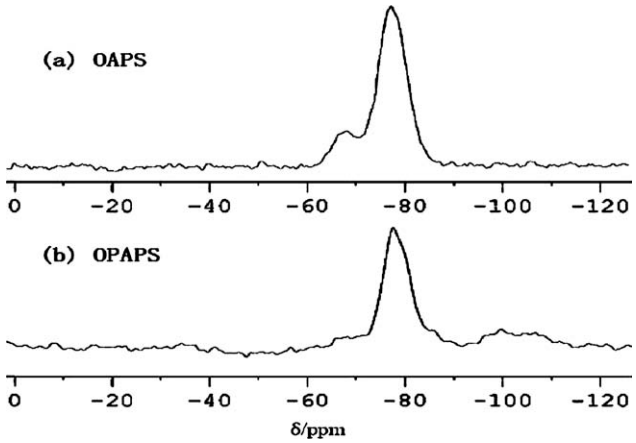

Figure 3. ^{29}Si solid NMR spectra of (a) OAPS and (b) OPAPS.

The X-ray diffraction (XRD) analysis was achieved using an XPERT-PRP diffractometer system; Cu Kα radiation was used with a copper target over the 2θ range of 5–60°.

High-performance liquid chromatography (HPLC) measurements were performed on an Elite P230 system, and visualized with ultraviolet light. Tetrahydrofuran (THF) was used as the mobile phase at a flow rate of 1.0 mL min^{-1}.

Gel permeation chromatography (GPC) measurements were performed on a Waters GPC system, using a Waters 2414 RI detector, Waters HT3, HT4, HT5 columns, a Waters 1515 pump and a Breeze 2 data capture unit. The system was calibrated using polystyrene (PS) standards and THF was used as the eluent, at a flow rate of 1.0 mL min^{-1}; the detection temperature was 40°C.

Thermal gravimetric analysis (TGA) was performed on a Netzsch 209 F1 thermal analyzer at a heating rate of 10°C min^{-1}, over the temperature range 40–800°C.

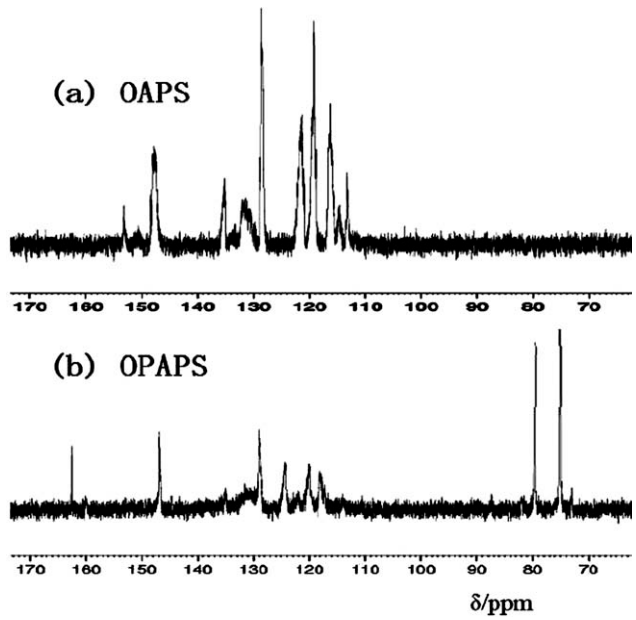

Figure 4. ^{13}C-NMR spectra of (a) OAPS and (b) OPAPS.

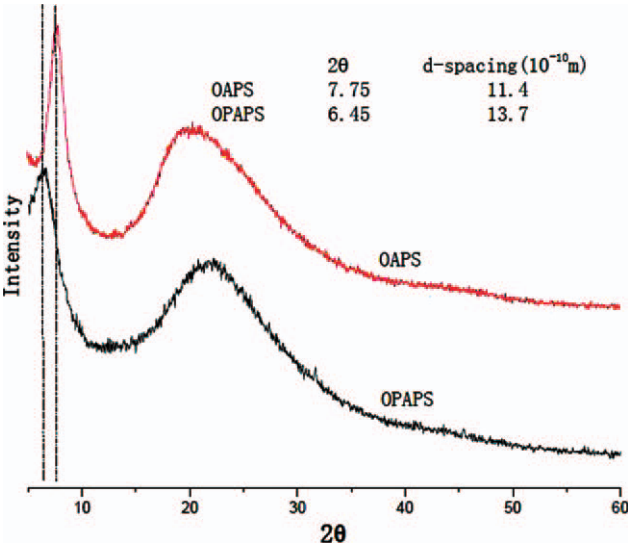

Figure 5. X-Ray diffraction patterns of OAPS and OPAPS. [Color figure can be viewed in the online issue, which is available at wileyonlinelibrary.com.]

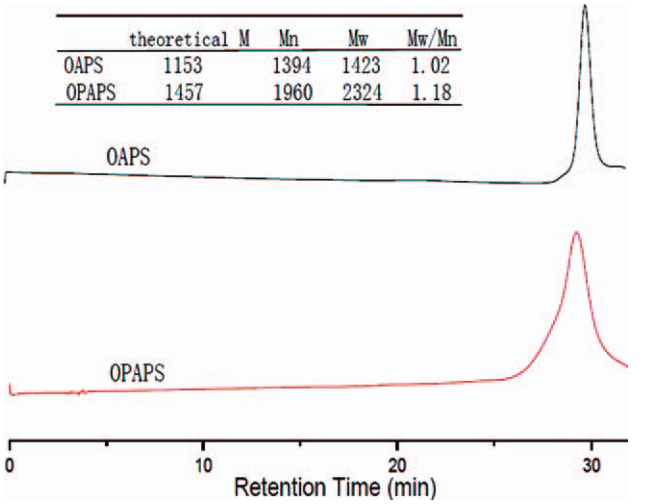

Figure 7. Gel permeation chromatography results for OAPS and OPAPS in THF at 40°C.[Color figure can be viewed in the online issue, which is available at wileyonlinelibrary.com.]

Elemental analyses were performed on a Flash EA 1112 automatic elemental analyzer.

DSC measurements were performed on a Netzsch DSC 204 F1 instrument (Germany). The DSC instrument was set for the temperature range 30–380°C. Heating rates of 5, 10, 15, and 20°C min^{-1} were chosen for the tests, under a nitrogen flow of 20 cm^3 min^{-1}.

RESULTS AND DISCUSSION

Synthesis and Characterization

To synthesize the OPAPS cube a simple synthetic strategy was used. The procedure reported by Laine et al.[32] for the synthesis of octa(nitrophenyl)silsesquioxane (ONPS) was improved upon. The result of this improved procedure was that every phenyl unit on ONPS had only one nitro group. Then ONPS was quantitatively transformed to OAPS by a hydrogen-transfer reduction in the presence of NH_2NH_2 and $FeCl_3$/C catalyst.[30,31] Finally, OPAPS was synthesized from OAPS with propargyl bromide in DMF. The product OPAPS can dissolve in most organic solvents, such as acetone, THF, DMF, and DMSO at room temperature. Its excellent solubility will be beneficial to its applicability in future.

The selection of the solvent plays an important role in increasing the conversion of the —NH_2 into —$NHCH_2C{\equiv}CH$. THF and ethylene glycol dimethyl ether are used for this type of reaction (OAPS reacted with —Br) in References 32 and 33. But the triethylaminehydrobromide by-product was not dissolved in THF and ethylene glycol dimethyl ether. Also triethylaminehydrobromide would adsorb some OAPS and OPAPS adhering to the beaker wall, which meant that the reaction could not proceed smoothly and resulted in a yield lower than 10% in our experiments. In this study, we used DMF to replace THF or ethylene glycol dimethyl ether because triethylaminehydrobromide

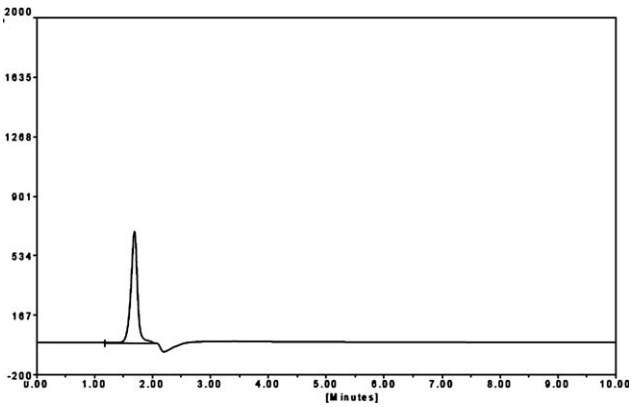

Figure 6. High-performance liquid chromatography traces for OPAPS.

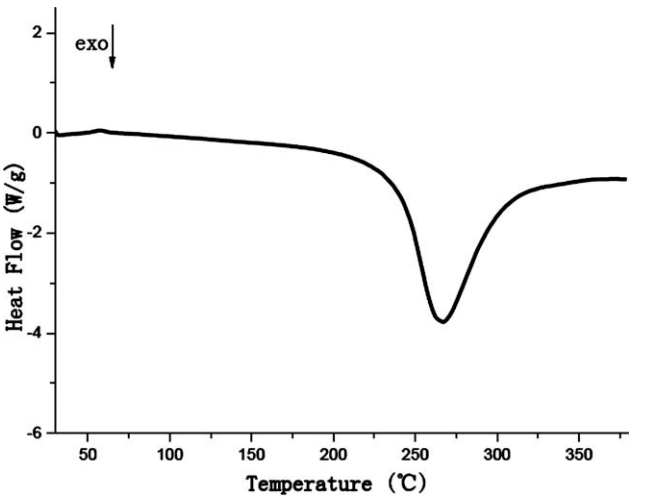

Figure 8. Differential scanning calorimetry curve of OPAPS at the heating rate of 10°C min^{-1} in N_2.

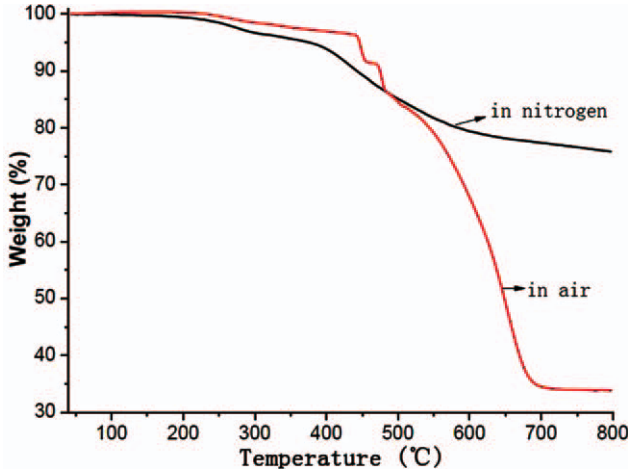

Figure 9. Thermal gravimetric analysis curves of OPAPS. [Color figure can be viewed in the online issue, which is available at wileyonlinelibrary.com.]

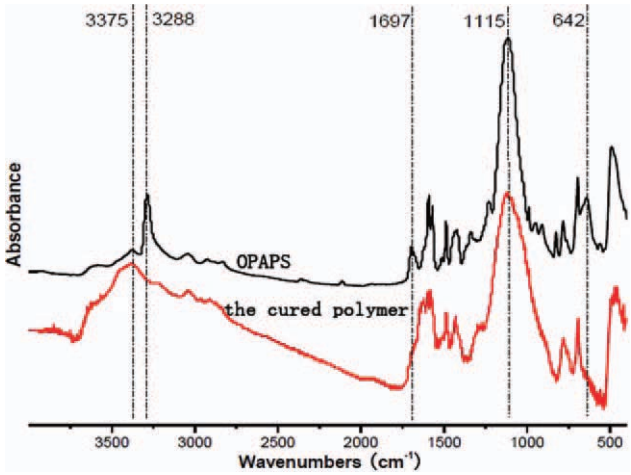

Figure 10. Fourier transform infrared spectra of OPAPS and the cured polymer (KBr). [Color figure can be viewed in the online issue, which is available at wileyonlinelibrary.com.]

can be dissolved in DMF. Then an aqueous saturated solution of NaCl was used as the precipitator. This was better than DMF in dissolving triethylaminehydrobromide to remove most of the by-product, and OPAPS was further purified by being dissolved in THF and ethyl acetate, then washed with the aqueous saturated solution of NaCl and precipitated in hexane. The yield was 82.4%.

FTIR spectra of OAPS and OPAPS are given in Figure 1. The FTIR spectrum of OAPS exhibited broad symmetric and asymmetric ν (N—H) peaks at 3358 and 3456 cm^{-1}, respectively.[30,32] These peaks disappeared completely and a new ν (—NH—) peak appeared at 3375 cm^{-1} in the FTIR spectrum of OPAPS. At the same time, the characteristic absorbance bands of —CH of terminal alkyne appeared at 3288, 1697, and 642 cm^{-1}. The 2113 cm^{-1} (—C≡C) peak was very small because of the symmetrical structure of OPAPS. It was noticeable that spectra for OAPS and OPAPS featured characteristic (Si—O—Si) stretching signals at 1115 cm^{-1} with relatively high intensity.

The structures of OAPS and OPAPS were confirmed by ^{1}H-NMR spectra (DMSO-d_6) (Figure 2). In Figure 2(a), the —NH_2 protons appear at 5.4–4.5 ppm and the aromatic protons appear at 7.4–6.2 ppm. The ratio of —NH_2 protons to aromatic C—H protons was 1:2.1, which corresponded to the structure of OAPS. The efficient transformation of OAPS to OPAPS was also evident from the ^{1}H-NMR spectra because the peak for the —NH_2 protons almost disappeared [Figure 2(b)]. Meanwhile, three new peaks were present, which were 4.1 ppm (—NH—), 3.9 ppm (—CH_2—) and 3.0 ppm (—C≡CH). Their presence supported the FTIR data.

Figure 3 shows the ^{29}Si solid NMR spectra of OAPS and OPAPS. Two peaks were observed at −77.5 and −68.3 ppm of OAPS corresponding to the isomers of para- and meta-NH_2 on the phenyl ring, respectively.[34] After the conversion of —NH_2 into —$NHCH_2C{\equiv}CH$, only one peak was observed at −77.8 ppm for OPAPS [Figure 3(b)], which was due to the alkyne weakening the electronic effect of —NH—. Hence, the different substitution isomers on the phenyl ring did not influence the electron cloud of Si.

Figure 4 shows the ^{13}C-NMR spectra of OAPS and OPAPS. All of the resonance peaks from 110 to 165 ppm were due to the C in the phenyl ring. In Figure 4(b), the two peaks of 79.5 and 75.1 ppm are from the C in —C≡CH. The ^{13}C-NMR was not

Table I. Thermal Gravimetric Analysis Results for OPAPS Under Different Atmospheres

Atmosphere	T_{d5} (°C)	Residual yield at 800°C (%)
Nitrogen	373.7	75.78
Air	446.4	33.81

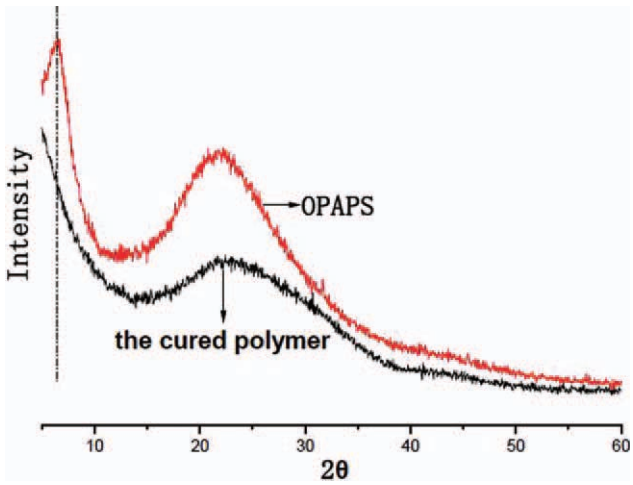

Figure 11. X-Ray diffraction patterns of OPAPS and the cured polymer. [Color figure can be viewed in the online issue, which is available at wileyonlinelibrary.com.]

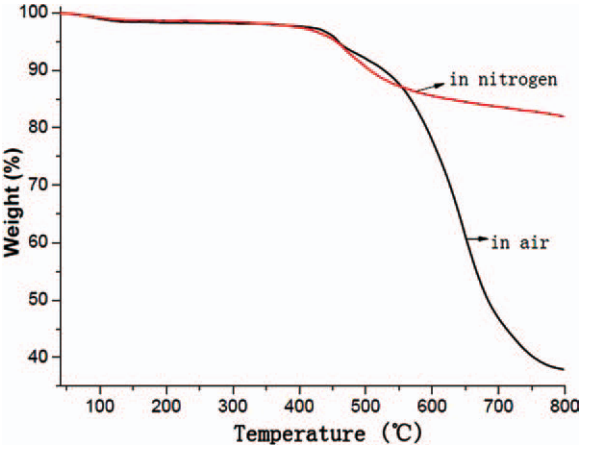

Figure 12. Thermal gravimetric analysis curves of the cured OPAPS polymer. [Color figure can be viewed in the online issue, which is available at wileyonlinelibrary.com.]

suitable for a quantitative analysis of carbon in different chemical environments.

The structure of OPAPS was also characterized by XRD (Figure 5). The XRD pattern of OAPS was similar to those in References 6 and 34. The XRD pattern of OPAPS in Figure 5 shows a wide amorphous diffraction peak. The diffraction peak of OAPS at $2\theta = 7.75°$ means a *d*-spacing of 11.4 Å (by Bragg's equation). At the same time, the XRD pattern of OPAPS shows a peak at $2\theta = 6.45°$ corresponding to a *d*-spacing of 13.7 Å. The diffraction peak is related to the local order of the POSS cage structure. The greater d-spacing of OPAPS indicates a bigger cage than that in OAPS.

The HPLC traces for OPAPS are shown in Figure 6. There is only one peak when the retention time is 1.69 min in Figure 6, which meant that OPAPS was of sufficient purity.

Table II. Thermal Gravimetric Analysis Results for the Cured OPAPS Polymer Under Different Atmospheres

Atmosphere	T_{d5} (°C)	Residual yield at 800°C (%)
Nitrogen	455.6	81.97
Air	458.8	37.90

Figure 7 shows the GPC of OAPS and OPAPS. The GPC revealed that the polydispersity index of OAPS was 1.02, confirming the purity of the OAPS and its stable cage structures. For OPAPS, there was only one peak which meant that all of the terminal alkynes did not polymerize to form any large molecules under the reaction conditions. However, the relative number average molecular weights of OAPS and OPAPS measured by GPC were much higher than the number of the theoretical molecular weights. The reason for this difference was probably that GPC measurement was based on PS as the standard, while the structures of POSS were considerably different from that of PS.

The DSC curve for OPAPS at a heating rate of 10°C min^{-1} in N_2 is shown in Figure 8. In the 200–320°C range, there was an exothermal process with a peak temperature at 267.0°C and 902.6 J g^{-1} of exothermal heat. This exothermal peak resulted from the polymerization of the terminal alkynes. The temperature range of the exothermic peak was higher than the common polymerization of the terminal alkynes,[2,24] because the steric hindrance of the reaction was bigger as a result of there being eight alkynes in every molecule of OPAPS.

The TGA curves of OPAPS in nitrogen and air atmospheres are presented in Figure 9. Table I lists TGA results for OPAPS under different atmospheres. We observed that the T_{onset} (373.7°C) of OPAPS at 5% weight loss in N_2 was 72.7°C lower than in air (446.4°C) because the presence of oxygen was beneficial to the polymerization of the terminal alkynes.

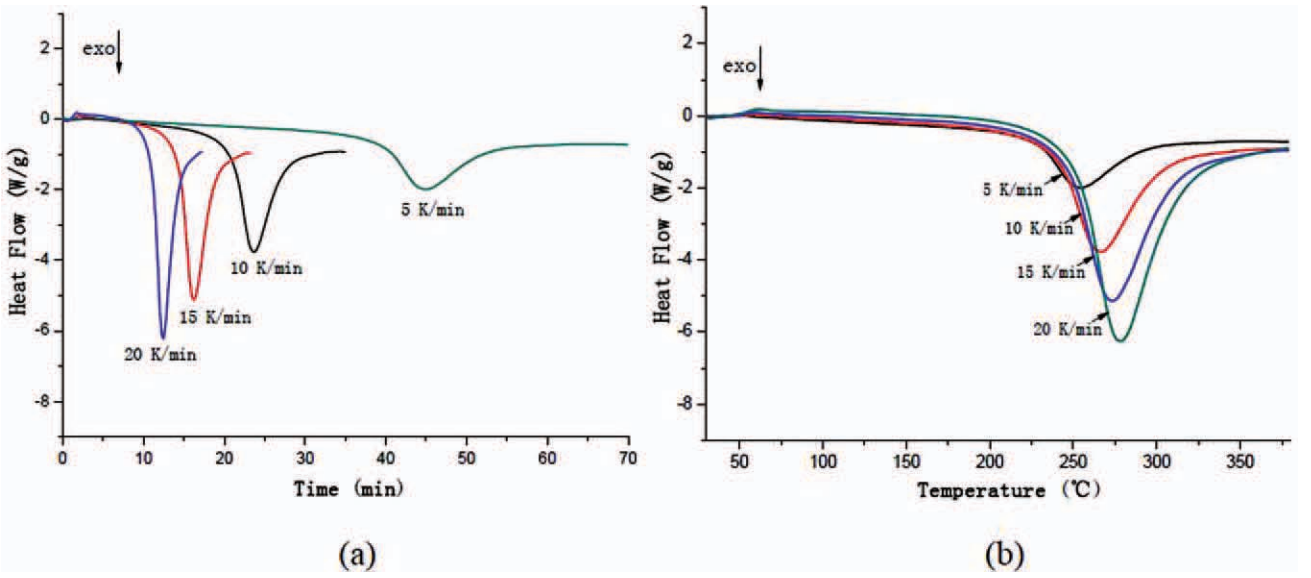

Figure 13. Heat flow versus the time (a) and temperature (b) at different heating rates. [Color figure can be viewed in the online issue, which is available at wileyonlinelibrary.com.]

Table III. Differential Scanning Calorimetry Analysis Results of OPAPS at Different Heating Rates

Heating rate ϕ (K min^{-1})	5	10	15	20
ΔH (J g^{-1})	883.1	902.6	899.3	838.3
T_p (°C)	254.4	267	273.3	278.2
α_p	41.00	43.06	40.91	40.74

And the residual yield at 800°C in N_2 atmosphere was much higher than the residue in air atmosphere due to the thermal oxidation.

Characterization of the Thermally Cured Polymer of OPAPS

According to the DSC curve in Figure 8, the curing reaction of OPAPS can take place in the 150–320°C temperature range. FTIR spectra of OPAPS and the thermally cured polymer of OPAPS are shown in Figure 10. As shown, the absorption peaks of —C≡CH (3288, 1697, and 642 cm^{-1}) disappeared after the thermal cure process, which means that the curing reaction of OPAPS was complete. At the same time, the absorption peaks of —NH— (3375 cm^{-1}) and Si—O (1115 cm^{-1}) were retained, which means the POSS structure was kept.

The structure of the thermally cured polymer of OPAPS was characterized by XRD (Figure 11). The result showed that the cured polymer was also an amorphous substance. Also the diffraction peak at $2\theta = 6.45°$ of OPAPS disappeared after the curing process, which meant that all of the POSS molecules had reacted and no single POSS molecule was existed.

The TGA curves of the thermally cured polymer of OPAPS in nitrogen and air atmospheres are presented in Figure 12. Table II lists TGA results for the cured OPAPS polymer under different atmospheres. The temperatures at 5% weight loss (T_{d5}) under different atmospheres were close. This indicated that the cured OPAPS polymer had good thermal-oxidative stability. The cured OPAPS polymer demonstrated

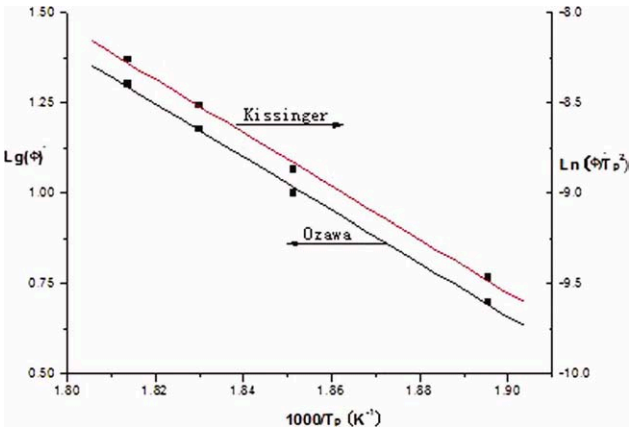

Figure 14. lg(ϕ) and ln(ϕ/T_p^2) as a function of the inverse of absolute temperature for the thermal curing reaction of OPAPS. [Color figure can be viewed in the online issue, which is available at wileyonlinelibrary.com.]

Table IV. Kinetic Parameters of the Thermal Curing Reaction of OPAPS

Methods	E_a (kJ mol^{-1})	Correlation coefficient R^2	A (10^{11} min^{-1})	N
Ozawa	133.8	0.9990		
Kissinger	122.7	0.9987	3.881	
Crane				0.87

the slow and steady degradation process in nitrogen. The rapid decomposition at ~ 550°C was steeper in air, and thus more rapid than in nitrogen. And the residual yield at 800°C in N_2 atmosphere was much higher than the residue in air atmosphere due to the presence of O_2. Comparing with the data in Table I, it was observed that the residual yield at 800°C of the cured OPAPS polymer in N_2 (81.97%) was 6.2% higher than the residual yield at 800°C of OPAPS in N_2 (75.78%) because of the polymerization of the terminal alkynes.

Investigation of Cure Kinetics of OPAPS

Dynamic DSC measurements for OPAPS were performed in the range of 30–380°C at the four heating rates of 5, 10, 15, and 20 K min^{-1} (Figure 13).[35–39] Figure 13(a), which shows the heat flow changes versus the time, was used to calculate the curing reaction heat by the method of integration. Figure 13(b) shows the heat flow changes versus the temperature. The exothermal heat ΔH, curing peak temperature T_p and conversion at peak α_p at each heating rate are listed in Table III. As shown in Figure 13(b), it can be observed that the curves shifted to higher temperature as the heating rate increased. The average cure reaction heat was 881 J g^{-1}.

The multiple heating rate methods for non-isothermal analysis proposed by Kissinger and Ozawa can be used to calculate the kinetic parameters of thermal curing reactions.[2,35] The logarithmic plots of heating rate ϕ versus the reciprocal of the absolute peak temperature for OPAPS are given in Figure 14. As shown, there is a good linear relationship between the logarithm of the heating rate and the inverse of the exothermic peak temperature. The values for the intercept and E_a calculated according to the Ozawa method were 33.70 and 133.8 kJ mol^{-1}, respectively. According to Figure 14, and using with the method of Kissinger,[35,37] an E_a of 122.7 kJ mol^{-1} and a frequency factor A of 3.881×10^{11} min^{-1} were obtained from the maximum reaction rate where $d(d\phi/dt)/dt$ was zero at a constant heating rate. The curing reaction order $n = 0.87$ was obtained by the Crane method.[37] The kinetic parameters for the thermal curing reaction of OPAPS are listed in Table IV.

CONCLUSIONS

A novel organic–inorganic hybrid polyhedral oligomeric octa (propargylaminophenyl) silsesquioxane (OPAPS, $(SiO_{1.5}C_6H_4NHCH_2C{\equiv}CH)_8$) was successfully synthesized. The chemical structure of OPAPS was characterized using FTIR, NMR, XRD, HPLC, GPC, DSC, and TGA. FTIR and ^{1}H-NMR revealed that almost all of the —NH_2 groups were changed to propargylaminophenyl groups. XRD suggested that OPAPS

was a kind of amorphous compound, and had a greater *d*-spacing than OAPS, demonstrating the larger POSS cage. There was only one peak in the HPLC traces for OPAPS, which signified that OPAPS was of sufficient purity. OPAPS was cured at a temperature in the range 150–320°C and the structure of the thermally cured polymer of OPAPS was characterized by FTIR, XRD, and TGA. It exhibited good thermal and thermal-oxidative stability. TGA demonstrated that the thermal decomposition temperatures (T_{d5}) of the cured OPAPS in nitrogen and air reached 455.6 and 458.8°C, respectively. The thermal curing reaction kinetics of OPAPS was studied by the Kissinger and Ozawa methods. Some curing reaction kinetic parameters were obtained, such as the reaction order n of 0.87, the apparent activation energy E_a of 122.7 kJ mol^{-1} according to the Kissinger method, and the frequency factor A of 3.881×10^{11} min^{-1}.

REFERENCES

1. Lickiss, P. D.; Rataboul, F. *Adv. Organomet. Chem.* **2008,** *57*, 1.
2. Li, Q.; Zhou, Y.; Huang, X. D.; Deng, S. F.; Huang, F. R.; Du, L.; Li.Z. P. *Eur. Polym. J.* **2008,** *44*, 2538.
3. Cordes, D. B.; Lickiss, P. D.; Rataboul, F. *Chem. Rev.* **2010,** *110*, 2081.
4. Gao, F.; Tong, Y. H.; Schricker, S. R.; Culbertson, B. M. *Polym. Adv. Technol.* **2001,** *12*, 355.
5. Ervithayasuporn, V.; Wang, X.; Gacal, B.; Gacal, B. N. *J. Organomet. Chem.* **2011,** *696*, 2193.
6. Zhang, J.; Xu, R. W.; Yu, D. S. *Eur. Polym. J.* **2007,** *43*, 743.
7. Chen, X. L.; Jiao, C. M. *Polym. Adv. Technol.* **2010,** *21*, 490.
8. Fina, A.; Tabuani, D.; Camiato, F.; Frache, A.; Boccaleri, E.; Camino, G. *Thermochim. Acta.* **2006,** *440*, 36.
9. Ak, M.; Gacal, B.; Kiskan, B.; Yagci, Y.; Toppare, L. *Polymer* **2008,** *49*, 2202.
10. Zhang, W. A.; Muller, A. H. E. *Macromolecules* **2010,** *43*, 3148.
11. Markovic, E.; Clarke, S.; Matisons, J.; Simon, G. P. *Macromolecules* **2008,** *41*, 1685.
12. Liu, H. Z.; Zheng, S. X.; Nie, K. M. *Macromolecules* **2005,** *38*, 5088.
13. Liu, H. Z.; Zheng, S. X. *Macromol. Rapid. Commun.* **2005,** *26*, 196.
14. Shimojima, A.; Goto, R.; Atsumi, N.; Kuroda, K. *Chem. Eur. J.* **2008,** *14*, 8500.
15. Feher, F. J.; Newman, D. A.; Walzer, J. F. *J. Am. Chem. Soc.* **1989,** *111*, 1741.
16. Feher, F. J.; Weller, K. J.; Schwab, J. *Organometallics* **1995,** *14*, 2009.
17. Duchateau, R.; Abbenhuis, H. C. L.; Santen, R. A. V.; Thiele, S. K. H.; Tol, M. F. H. A. *Organometallics* **1998,** *17*, 5222.
18. Zhang, Y. W.; Ye, Z. B. *Chem. Commun.* **2008,** 1178.
19. Carniato, F.; Bisio, C.; Boccaleri, E.; Guidotti, M.; Garilova, E.; Marchese, L. *Chem. Eur. J.* **2008,** *14*, 8098.
20. McCusker, C.; Carroll, J.; Rotello, V. M. *Chem. Commun.* **2005,** 996.
21. Liu, H. Z.; Kondo, S.; Tanaka, R.; Oku, H.; Unno, M. *J. Organomet. Chem.* **2008,** *693*, 1301.
22. Bassindale, A. R.; Pourny, M.; Taylor, P. G.; Hursthouse, M. B.; Light, M. E. *Angew. Chem.* **2003,** *115*, 3612.
23. Wright, M. E.; Schorzman, D. A.; Feher, F. J.; Jin, R. Z. *Chem. Mater.* **2003,** *15*, 264.
24. Gao, F.; Zhang, L. L.; Tang, L. M.; Zhang, J.; Zhou.Y.; Huang, F. R.; Du, L. *Bull. Korean. Chem. Soc.* **2010,** *31*, 976.
25. Wu, S. M.; Hayakawa, T.; Kikuchi, R.; Grunzinger, S. J.; Kakimoto, M. A. *Macromolecules* **2007,** *40*, 5698.
26. Itoh, A.; Inoue, K.; Iwata, K.; Mitsuzuka, M.; Kakigano, T. *Macromolecules* **1997,** *30*, 694.
27. Wang, F.; Zhang, J.; Huang, J. X.; Yan, H.; Huang, F. R.; Du, L. *Polym. Bull.* **2006,** *56*, 19.
28. Qin, A. J.; Jim, C. K. W.; Lu, W. X.; Lam, J. W. Y.; Haussler, M. *Macromolecules* **2007,** *40*, 2308.
29. Asuncion, M. Z.; Roll, M. F.; Laine, R. M. *Macromolecules* **2008,** *41*, 8047.
30. Zhang, J.; Xu, R. W.; Yu, D. S. *J. Appl. Polym. Sci.* **2007,** *103*, 1004.
31. Du, J. K. Doctoral Dissertation of Beijing Institute of Technology **2006.**
32. Tamaki, R.; Tanaka, Y.; Asuncion, M. Z.; Choi, J.; Laine, R. M. *J. Am. Chem. Soc.* **2001,** *123*, 12416.
33. Hussain, H.; Tan, B. H.; Gudipatl, C. S.; Xaio, Y.; Liu, Y.; Davis, T. S.; He, C. B. *J. Polym. Sci. Polym. Chem.* **2001,** *46*, 7287.
34. Nagendiran, S.; Alagar, M.; Hamerton, I. *Acta. Meter.* **2010,** *58*, 3345.
35. Hayaty, M.; Beheshty, M. H.; Esfandeh, M. *J. Appl. Polym. Sci.* **2011,** *120*, 62.
36. Dupuy, J.; Leroy, E.; Maazouz, A. *J. Appl. Polym. Sci.* **2000,** *78*, 2262.
37. Luo, Y. H.; Hu, Y. H.; Wan, L. Q.; Xue, L. *Chem. J. Chinese. U.* **2006,** *27*, 170.
38. Sastri, S. B.; Keller, T. M.; Jones, K. M.; Armistead, P. *Macromolecules* **1993,** *110*, 6171.
39. Alonso, M. V.; Oliet, M.; Perez, J. M.; Rodriguez, F.; Echeverria, J. *Thermochim. Acta.* **2004,** *419*, 161.